


# Synthesis and Properties of Vermiculite-Reinforced Polyurethane Nanocomposites

Yuqiang Qian,<sup>†</sup> Chris I. Lindsay,<sup>‡</sup> Chris Macosko,<sup>§,\*</sup> and Andreas Stein<sup>†,\*</sup>

<sup>†</sup>Department of Chemistry, University of Minnesota, 207 Pleasant St. SE, Minneapolis, Minnesota 55455, United States

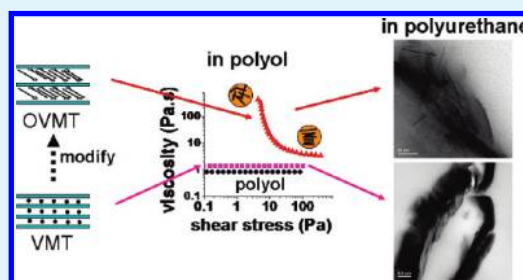
<sup>‡</sup>Huntsman Polyurethanes, Everslaan 45, 3078 Everberg, Belgium

<sup>§</sup>Department of Chemical Engineering & Materials Science, University of Minnesota, 421 Washington Ave. SE, Minneapolis, Minnesota 55455, United States

 Supporting Information

**ABSTRACT:** Natural vermiculite was modified by cation exchange with long-chain quaternary alkylammonium salts and then dispersed in polyether-based polyols with different structures and ethylene oxide/propylene oxide ratios. The dispersions were evaluated by X-ray scattering and rheology. In all polyol dispersions tested, polyols were intercalated into the vermiculite interlayers. Also, significant shear thinning behavior was observed. A large interlayer spacing of  $\sim 90$  Å was achieved in one polyol suitable for polyurethane elastomer synthesis. In polyurethane made with this polyol, clay platelets were extensively intercalated or exfoliated. The composites showed a  $>270\%$  increase in tensile modulus,  $>60\%$  increase in tensile strength, and a 30% reduction in  $N_2$  permeability with a loading of 5.3 wt % clay in polyurethane. Differential scanning calorimetry and dynamic mechanical analysis revealed that the nanoclay interacts with the polyurethane hard segments.

**KEYWORDS:** vermiculite, organoclay, polyurethane, elastomer, polymer–clay nanocomposites, barrier properties



## INTRODUCTION

Polyurethane (PU) is one of the most versatile polymers. By changing the type and functionality of the polyol and isocyanate precursors, the properties of PU can be easily tailored, ranging from rigid solid to flexible elastomer. PU elastomers have been widely used as coatings, adhesives, and foams because of their excellent flexibility, elasticity, and damping ability.<sup>1</sup> The mechanical properties can be further improved by incorporation of a variety of fillers, such as clays,<sup>2,3</sup> glass or carbon fibers,<sup>4,5</sup> carbon nanotubes,<sup>6</sup> and graphene sheets<sup>7</sup> into PU formulations.

In particular, clays and layered silicate minerals have been extensively studied as low-cost fillers to enhance the mechanical and physical properties of polymer composites.<sup>2,3,8–10</sup> The property enhancement is especially pronounced, even at relatively low filler loadings, when highly exfoliated clay sheets are dispersed within the polymer matrix, forming polymer–clay nanocomposites. This effect was discovered by Toyota researchers studying nylon-6 composites in the 1980s,<sup>8</sup> and since then, a number of polymers have been reported to exhibit similar reinforcement when nanocomposites with clay are formed. PU elastomer–clay nanocomposites were first reported by Pinnavia et al., who showed that montmorillonite modified by long-chain alkylammonium cations could be solvated by polyols and that the final composites exhibited improved tensile properties.<sup>2</sup> Different types of polyols,<sup>11</sup> organomodifiers,<sup>12,13</sup> and processing techniques<sup>14</sup> have been studied for preparing elastomeric PU nanocomposites. In situ polymerization is widely employed to

form nanocomposites by intercalating the monomers or pre-polymers into the clay interlayer spacing before adding curing agents.<sup>2,3,11,12,15</sup> Mechanical properties, flammability, and barrier properties of polyurethane clay composites have also been investigated extensively.<sup>15–20</sup> The incorporation of well-dispersed clay nanosheets into polymer matrices increases the tensile modulus and tensile strength in most of cases,<sup>15,16</sup> and a delay in heat release during combustion is also observed.<sup>17,18</sup> As high-aspect-ratio nanofillers, clays also reduce the gas and water vapor permeability rate in PU coatings or films.<sup>19,20</sup>

Interestingly, in spite of the broad selection of available clays, most studies of PU clay composite have focused on montmorillonite, and only few consider other types of clay minerals, like mica,<sup>21,22</sup> kaolin<sup>23</sup> and laponite.<sup>24</sup> One clay of potential interest is vermiculite. Just like montmorillonite, vermiculite is a 2:1 phyllosilicate, in which the negatively charged aluminosilicate layer is composed of one octahedral sheet sandwiched between two tetrahedral sheets. Magnesium and iron sites are also present within the sheets of typical vermiculites.<sup>25,26</sup> In addition, metal cations, mainly hydrated  $Mg^{2+}$  for natural vermiculite, are located between the layers to balance the charge. Compared with montmorillonite, the clay sheets in vermiculite have a higher charge density, a key parameter facilitating the incorporation

**Received:** July 7, 2011

**Accepted:** August 19, 2011

**Published:** August 19, 2011

of cationic organic modifiers to generate larger interlayer spacings.<sup>27</sup> Vermiculite forms macroscopic crystals, that are potentially suitable for producing high-aspect-ratio nanofillers, and its natural abundance makes it economically attractive for industrial applications. Although vermiculite is widely used as a packaging or adsorbing material, only few studies have focused on vermiculite-reinforced polymer composites.<sup>25,26,28–33</sup>

To facilitate nanocomposite formation, interlayer metal ions in clay can be exchanged with quaternary alkyl ammonium ions, rendering the clay surface more organophilic. Solvents, such as dimethylformamide or tetrahydrofuran, are commonly used to help swell the organoclay to facilitate intercalation of monomers or polymer chains or to conduct the synthesis of PU nanocomposites. However, the resulting composites have a high content of volatile organic compounds, and the removal of solvents adds to the processing cost. For thermoset polymers, the solvent can be trapped in the cross-linked network and complete removal of solvent can be hard to achieve. Therefore, the presence of organic solvents limits applications, and it is worthwhile to study syntheses of composites formed in situ without using any organic solvent.

In this work, natural vermiculite was modified with two types of organomodifiers and dispersed in polyether-based polyols, and then solvent-free polymerization was carried out to synthesize PU-vermiculite nanocomposites. Polyols with different ethylene oxide (EO) to propylene oxide (PO) ratios were used to study the swelling behavior of organovermiculite (OVMT). The polyol with the best swelling capability was chosen for the PU composite synthesis, in which both pristine and organo-modified vermiculites were used for comparison. The extent of clay exfoliation in the final composites was characterized by X-ray scattering and electron microscopy. Thermal, mechanical, and gas barrier properties of the composites were also evaluated.

## EXPERIMENTAL SECTION

**Materials.** Natural vermiculite (Grade 3, Sigma-Aldrich, thermally expanded at 650 °C) was jet-milled (Hosokawa Micron, UK) to a particle size less than 4 μm before use. Sodium chloride (VMR Inc.), cetyltrimethylammonium bromide (CTAB, 99%, Sigma) and octadecyl bis(hydroxyethyl)methylammonium chloride (OBMAC, 90%, Faen

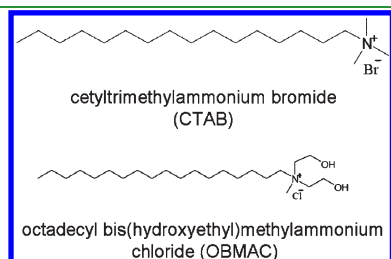


**Figure 1.** Chemical structures of the CTAB and OBMAC modifiers.

**Table 1.** Specifications of the Polyols Selected in This Study

notation	polyol trade name	functionality	mol wt	composition <sup>a</sup>
PL1	Daltocel F555	3	6000	EO tipped, central EO/PO random copolymer, overall EO/PO=75/25
PL2	Jeffol G31-28	3	6000	15% EO tipped, central all PO
PL3	Jeffol PPG-2000	2	2000	All PO

<sup>a</sup>EO tipped refers to the PEO block at the end of the polyol chains, leaving a primary hydroxyl group.

Industry Co., Shandong, China) were used as received to modify vermiculite (Figure 1). Methylene diphenyl diisocyanate (MDI, Suprasec 3050, Huntsman Polyurethanes, 1:1 mixture of 2,4'- and 4,4'-MDI), silicone defoamer (BYK-88, BYK), and amine catalyst (Dabco S-25, Air Products) were used as received. 1,4-butanediol (BDO, ≥ 99%, Sigma-Aldrich) was dried under vacuum before use.

Three polyether-based polyols for PU elastomers were used. Their properties, provided by Huntsman Polyurethanes, are listed in Table 1.

**Modification of Vermiculite.** The jet-milled vermiculite (VMT) was modified according to a method reported elsewhere.<sup>34</sup> Vermiculite powder (20 g) was dispersed in 100 mL of 4 M NaCl solution and the mixture was refluxed for 2 days. The exchange was carried out twice using fresh NaCl solution to replace interlayer ions by Na<sup>+</sup> more completely. The product was separated by centrifugation and washed several times with deionized water and ethanol until it was Cl<sup>-</sup>-free (tested using a 0.1 M AgNO<sub>3</sub> solution), then dried overnight in a vacuum oven at 90 °C. OVMT was synthesized by exchanging Na-VMT with the organomodifier solution, which contained excess CTAB or OBMAC (120% of the measured effective cation exchange capacity (CEC) of Na-VMT), at 80 °C for 2 days. The exchange was repeated for a second time, and the product was separated by centrifugation, washed until it was halide-free, and dried under a vacuum at 90 °C overnight. The organomodified VMTs were denoted CTAB-VMT or OBMAC-VMT, respectively.

**Dispersion of VMT in Polyols.** Different amounts of CTAB-VMT and OBMAC-VMT were added to the polyols to form dispersions with 2.0, 3.8, or 7.4 wt % clay. The mixtures were stirred at 2000 rpm for 30 min and then subjected to probe ultrasonication (5 mm tapered microtip, 25% amplitude, VCX-750 ultrasonic processor, Cole Parmer) for 30 min (2 s sonication/2 s rest, *T* < 60 °C) while being magnetically stirred.

**Synthesis of PU and PU-VMT Nanocomposites.** A formulation of a PU with 30% hard block is listed in Table 2. Polyol or polyol-VMT dispersions were dried under vacuum at 90 °C for at least 3 h before use. The defoamer (BYK-88) and 1,4-butanediol were added to the polyol dispersion, which was then mixed at ~500 rpm and vacuum degassed. The desired amount of diisocyanate was added, and the blend was mixed at ~300 rpm for 2 min followed by vacuum degassing. Catalyst (Dabco S-25) was added dropwise with gentle hand mixing. For the composites with 2.7 and 5.3 wt % OVMT, no catalyst was added. When the mixture began to heat up, it was poured on a high-density polyethylene (HDPE) plate and covered with another HDPE plate to minimize exposure to moisture and to control the film thickness. The polymer was cured at room temperature for 1 day and then at 100 °C for 2 days. The resulting composites were denoted as PU\_X-VMT\_Y (*X* is the modifier, *Y* is the clay weight percentage in the final composite).

**Characterization.** X-ray diffraction (XRD) patterns were acquired using a PANalytical X-Pert Pro MPD X-ray diffractometer equipped with a Co source (45 kV, 40 mA, λ = 1.790 Å) and an X-Celerator detector. X-ray scattering patterns of the polyol dispersions and PU composites were acquired on a Rigaku RU-200BVH 2D SAXS instrument with a Cu X-ray source (45 kV, 40 mA, λ = 1.542 Å) and a Siemens Hi-Star multiwire area detector with sample-to-detector distances of 58 cm for the polyol dispersions and 30 cm for the PU composites.

Table 2. Formulation of the PU Elastomer

ingredient	parts by weight
polyol (Jeffol G31-28)	70
1,4-butanediol	6.54
MDI (Suprasec 3050)	23.38
defoamer (BYK-88)	0.5
catalyst (Dabco S-25)	<0.15

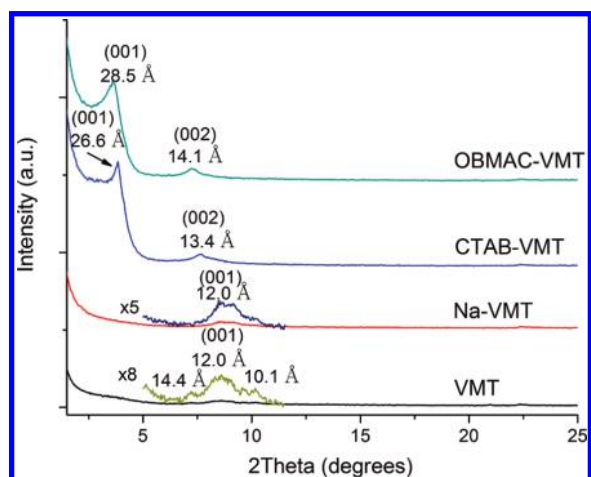


**Figure 2.** XRD patterns of vermiculite samples before and after modification. XRD traces are offset for comparison. The intensities of the VMT and Na-VMT peaks are relatively low because the same narrow slit was used during data collection as for the other two samples, whose low-angle features required use of a narrow slit to avoid oversaturation of the detector.

Fourier transform-infrared (FT-IR) spectroscopy was carried out using a Nicolet Magna-IR 760 spectrometer. Compositions of clay samples were analyzed using a Thermo Scientific iCAP 6500 dual-view, inductively coupled plasma-optical emission spectrometer (ICP-OES). Transmission electron microscopy (TEM) images were obtained on a FEI Tecnai T12 microscope using an accelerating voltage of 100 kV. Samples were cryo-microtomed (Leica Ultracut) at  $-100\text{ }^{\circ}\text{C}$  into 100 nm sections before being picked up on carbon-coated Cu grids. Thermogravimetric analyses were carried out with a Netzsch STA 409 PC instrument in air for the modified clay and with a Perkin-Elmer Pyris Diamond TG/DTA 6300 in nitrogen for the PU composites, using a ramping rate of  $10\text{ }^{\circ}\text{C}/\text{min}$ . Differential scanning calorimetry (DSC) measurements were carried out with a TA Instruments DSC Q1000. Thermal history was removed at  $200\text{ }^{\circ}\text{C}$ , and scans were performed from  $-100$  to  $200\text{ }^{\circ}\text{C}$  at a heating rate of  $10\text{ }^{\circ}\text{C}/\text{min}$ . Rheological properties of the polyol dispersions were measured using a TA Instruments AR-G2 rheometer with a 40 mm cone plate. Viscosity profiles were obtained under steady state flow as the shear rate was increased in logarithmic increments from  $0.01$  to  $100\text{ s}^{-1}$ . Tensile moduli were measured using a Rheometric Solid Analyzer-II with  $3\text{ mm} \times 3\text{ cm}$  sample strips. Dynamic sweeps at  $1\text{ rad/s}$  with a pretension of 1% strain were performed at room temperature to accurately determine the modulus, and the temperature dependence of the modulus was determined by a temperature ramp from  $-100$  to  $150\text{ }^{\circ}\text{C}$ . Ultimate tensile strength and the hysteresis were measured on a Rheometric Scientific Minimat using dumbbell-shaped samples ( $5\text{ mm}$  gauge length and  $2.6\text{ mm}$  width) at 100% strain per second. The hysteresis loss was determined as the area between the hysteresis loop divided by the area below the loading curve, and the permanent set was determined as the strain at zero stress in the unloading curve after the

Table 3. Weight Loss and Organic Contents of VMT and OVMT

sample	weight loss (%)	organic content from TGA (%)	organic content from CEC calculation (%)
VMT	3.6		
CTAB-VMT	25.1	22.3	22.4
OBMAC-VMT	27.8	25.1	27.4

fifth cycle. Gas permeation measurements were performed with a homemade manometric permeation cell.<sup>35</sup> Both the upstream and downstream pressures were maintained at 40 psi initially before the valve at the downstream side was quickly opened to ambient pressure and then closed. The pressure change on both sides was then monitored and converted to the permeability coefficient of the test gas.<sup>35</sup>

## RESULTS AND DISCUSSION

**Modification of Vermiculite.** The vermiculite used in this study was a hydrated magnesium aluminum iron silicate. It contained mixed divalent and monovalent interlayer cations as revealed by ICP-OES elemental analysis (see Table S1 in the Supporting Information), and the exchangeable cations were replaced by  $\text{Na}^+$  by refluxing in 4 M NaCl solution for 2 days. The amount of  $\text{Na}^+$  in the cation-exchanged product is directly related to the CEC of the vermiculite. Under the exchange conditions used here, the CEC of Na-VMT was calculated to be 99 mequiv/100 g on the basis of the  $\text{Na}_2\text{O}$  wt% in Na-VMT. After ion exchange with CTAB to form CTAB-VMT, almost all  $\text{Na}^+$  was exchanged, corresponding to a CEC value of 79 mequiv/100 g of CTAB-VMT. There were also slight decreases in the  $\text{Mg}^{2+}$  and  $\text{K}^+$  contents, assuming that the relative content of  $\text{SiO}_2$  did not change.

XRD was also used to monitor the exchange process. As can be seen from Figure 2, pristine vermiculite shows a major broad peak at  $d = 12.0\text{ }\text{\AA}$  and a weaker peak at  $d = 14.4\text{ }\text{\AA}$ , corresponding to the layer spacings of vermiculite in the mono- and double-hydrated  $\text{Mg}^{2+}$  forms, respectively.<sup>36</sup> Another peak at  $10.1\text{ }\text{\AA}$  could result from mica (biotite) impurities, as suggested from previous reports.<sup>37</sup> Vermiculite can form interstratified structures with other clays, such as biotites, and the random distribution of vermiculite layers causes peak broadening.<sup>38</sup> Na-VMT also exhibits a major peak at  $d = 12.0\text{ }\text{\AA}$ . Incorporation of alkyl-ammonium ions generates a  $d_{001}$ -spacing of  $26.6\text{ }\text{\AA}$  for CTAB-VMT and  $28.5\text{ }\text{\AA}$  for OBMAC-VMT. Compared with montmorillonite modified with similar modifiers,<sup>12</sup> the  $d_{001}$ -spacing of OVMT is larger, which may be related to closer packing of interlayer alkyl chains with a paraffin-type configuration in the OVMT.<sup>27</sup>

The presence of organic groups in OVMT was confirmed by FT-IR spectroscopy (see Figure S1 in the Supporting Information), and the organic content of OVMT was determined by thermogravimetric analysis in air by comparing its response curve up to  $900\text{ }^{\circ}\text{C}$  to that of VMT. The weight loss below  $150\text{ }^{\circ}\text{C}$  was due to surface-adsorbed water, so the weight loss from  $160$  to  $860\text{ }^{\circ}\text{C}$  was used to determine the content of organic components in OVMT by the following equation

$$\text{WL(OVMT)} = \text{OC wt\%} + \text{VMT wt\%} \times \text{WL(VMT)}$$

where  $\text{WL(OVMT)}$  and  $\text{WL(VMT)}$  are the weight loss values of OVMT and VMT, respectively, and  $\text{OCwt\%}$  and  $\text{VMTwt\%}$  are the relative contents of the organic component and the inorganic



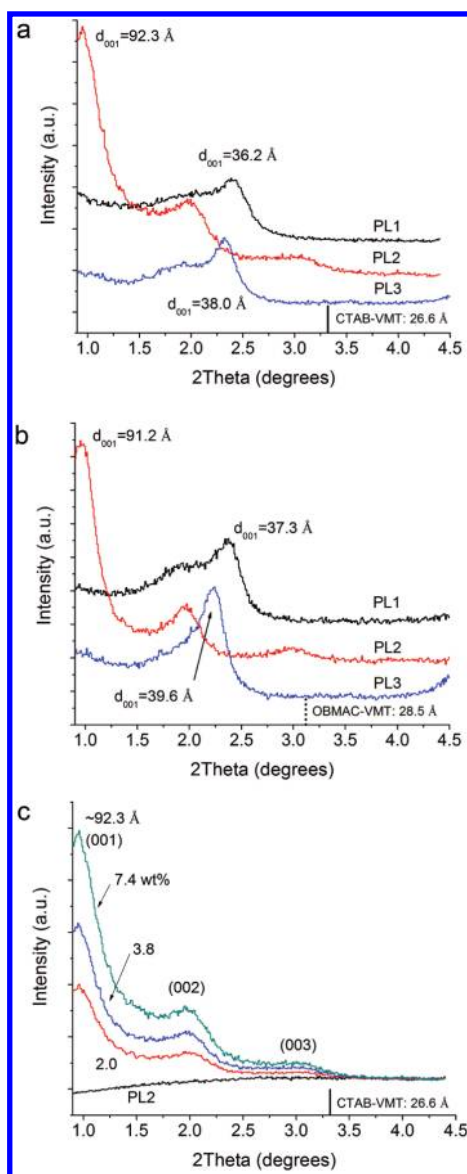


**Figure 3.** X-ray scattering patterns of polyol dispersions with 3.8 wt % of (a) CTAB-VMT, (b) OBMAC-VMT, and (c) PL2 dispersions with different contents of CTAB-VMT.

vermiculite component, respectively. The weight losses of pristine and organomodified vermiculites are listed in Table 3, which also tabulates the organic contents calculated from both TGA results and CEC estimations. CTAB-VMT has an organic content of 22.3%, slightly lower than that of OBMAC-VMT, mainly because of the difference in molecular weights of the two modifiers (see structures in Figure 1). Both values are close to the corresponding calculated values based on the CEC, which indicates nearly complete exchange of  $\text{Na}^+$  with CTAB or OBMAC.

**Polyol-VMT Dispersions.** Probe sonication proved to be effective in dispersing clay particles in polyol, producing homogeneous dispersions. Whereas VMT dispersions showed some sedimentation with time, the appearance of CTAB-VMT dispersions did not change over a period of six weeks (see Figure S2 in the Supporting Information). Formation of a good polymer–clay nanocomposite by in situ polymerization requires intercalation

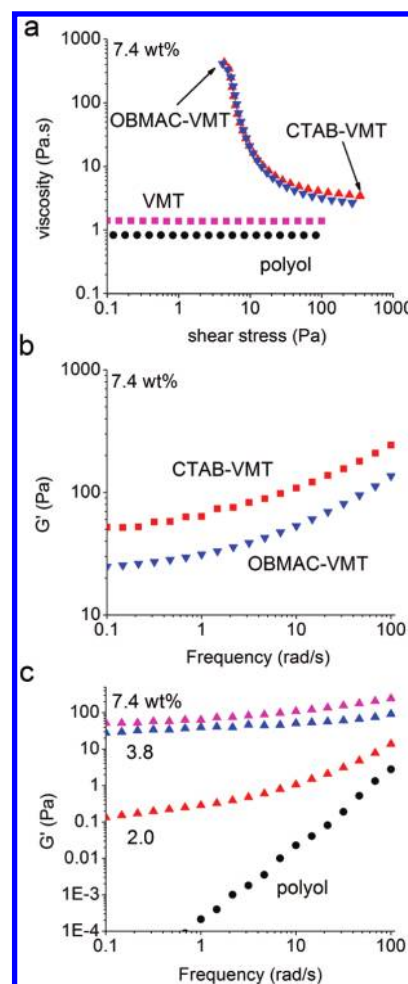


**Figure 4.** (a) Viscosity profiles of polyol dispersions with 7.4 wt % VMT and OBMAC-VMT dispersions. (b) Dynamic frequency sweep of PL2 dispersions with 7.4 wt % CTAB-VMT and OBMAC-VMT. (c) Concentration dependence of storage shear modulus of PL2 dispersions with CTAB-VMT.

of the monomer into the clay interlayer space, followed by expansion and exfoliation of the clay sheets as polymer chains grow during the polymerization process. The intercalation step is highly dependent on the compatibility between the monomer or prepolymer and the interlayer modifier. Once intercalation begins, the clay layer spacing increases. As can be seen from the X-ray scattering patterns in Figure 3a,b, all of the polyols tested here can be intercalated into the clay and increase the  $d$ -spacing to different levels. CTAB-VMT swells to 36.2 Å in PL1, the most hydrophilic polyol, and to 38.0 Å in PL3, the most hydrophobic one, whereas in PL2, the  $d$ -spacing is increased to 92.3 Å, i.e., several times larger than the original clay  $d$ -spacing (26.6 Å). OBMAC-VMT showed a similar behavior and also exhibited the largest  $d$ -spacing in PL2 dispersion. The EO/PO segments in the polyol have been reported to affect the intercalation of polyol in clay.<sup>39,40</sup> The EO tips help the polyol to access the interlayer space. In addition, the intercalation is affected by the structure of the polyol. PL1 has a random EO/PO central block, and due to the large content of EO (75% overall), the chain is slightly hydrophilic and interacts more with the clay surface. PL3 is composed of only PO, so except for the few –OH end-groups that interact with the clay surface, the PO chain mainly interacts with the interlayer modifier. PL2 contains 15% EO end groups that interact

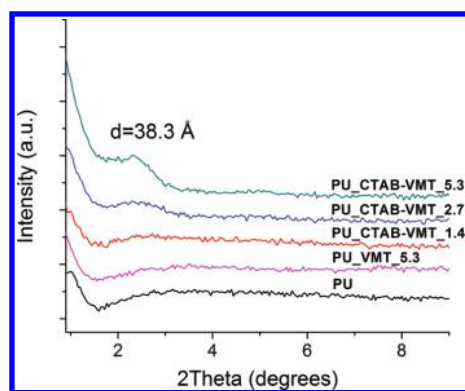


**Figure 5.** X-ray scattering patterns of neat PU and PU-VMT composites prepared from PL2.

strongly with the clay surface. The less polar PO blocks (85%) interact strongly with the organomodifier, causing increased expansion of the interlayer spacing upon intercalation. The distinct EO-PO-EO block structure makes PL2 similar to the Pluronic series of amphiphilic surfactants, which has been widely used as soft templates to synthesize mesoporous materials,<sup>41</sup> and a dispersion of CTAB-VMT in Pluronic P123 showed a similar spacing (see Figure S3 in the Supporting Information). It is therefore reasonable to propose that PL2 adopts a lamellar structure with EO on the surface and PO in the center. Figure 3c clearly shows that X-ray scattering intensity, but not spacing, increases with the concentration of CTAB-VMT in PL2.

The polyol-VMT dispersions were also characterized by rheology. Viscosity profiles for all three polyols can be found in the Supporting Information (Figure S4). The analysis was focused on dispersions in PL2 because it produced the largest extent of swelling. Figure 4a shows the viscosity of PL2 dispersions with 7.4 wt % of VMT and OVMT. With OVMT, the dispersion showed strong shear thinning, whereas Newtonian behavior was observed for neat polyol and the dispersion with VMT. Shear-thinning resulted from swelling of OVMT by the polyol and from a 3D network of clay sheets within the polyol matrix. Another indication of the formation of a solid-like network is that the storage shear modulus,  $G'$ , becomes nearly independent of frequency even at 2.0 wt % (Figure 4c) for PL2\_CTAB-VMT dispersions.  $G'$  can be used to evaluate the strength of the network. Figure 4b shows that  $G'$  of a PL2\_CTAB-VMT dispersion is twice as large as for a PL2\_OB-MAC-VMT dispersion with the same content of OVMT (7.4 wt %), indicating CTAB-VMT forms a stronger network in PL2 and thus a better dispersion.

As mentioned above, the intercalation of reactive monomers into the interlayer space of a clay is affected by the interlayer spacing, and a larger spacing can increase intercalation and can also facilitate the exfoliation of clay platelets as the chain grows during polymerization. Therefore, guided by the above X-ray scattering and rheological data, we chose the PL2\_CTAB-VMT system to synthesize PU composites and to study the effect of vermiculite addition on the properties of PU elastomers.

**PU-VMT Elastomer Nanocomposites.** Figure 5 shows the X-ray scattering patterns of neat PU and composites prepared from PL2. The absence of scattering peaks from the clay fillers is often considered to be a good indication of exfoliation. However, this applies only if the scattering signal of the original clay is reasonably strong and the concentration is above the detection

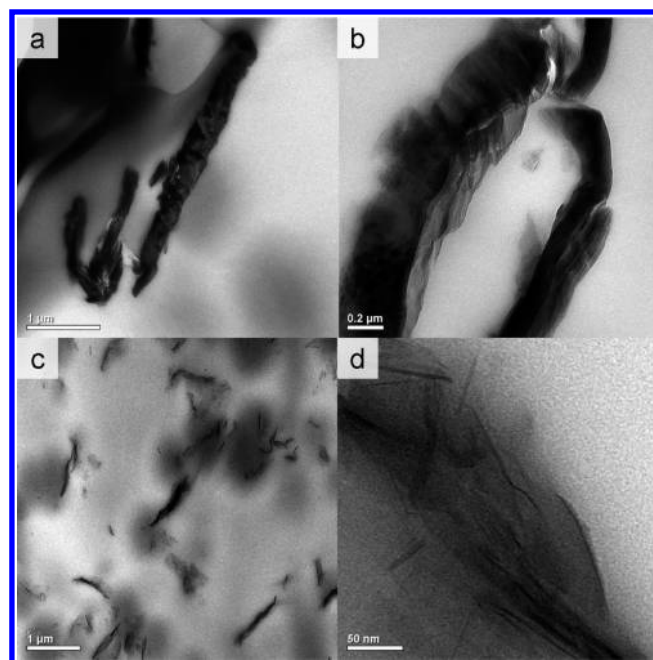


**Figure 6.** TEM images of PU composites (a, b) with VMT at 1.4 wt %, (c, d) with CTAB-VMT at 1.4 wt %.

limit. For the composite with CTAB-VMT, the scattering peak at  $2.3^\circ 2\theta$  is assigned to the clay, and it starts to be observable with at least 2.7 wt % of clay, corresponding to a  $d$ -spacing of 38.3 Å. It is worth noting that even though polyol PL2 can swell CTAB-VMT to a  $d$ -spacing of 92.3 Å, after polymerization, the change in surrounding environment (polyol to PU) caused a shrinkage of the swelled clay structure ( $d$ -spacing of 38.3 Å). Nevertheless, the  $d$ -spacing of clay in the composites is larger than that observed for the CTAB-VMT by itself ( $d$ -spacing of 26.6 Å). This is attributed to the intercalation of polymer chains, and the broadness of the peak suggests partial exfoliation and random expansion of clay platelets. In contrast, for the VMT composites, no scattering peaks were observed because of the weak scattering contribution of VMT, as shown in Figure 2.

TEM analysis was used as a complementary tool to characterize the state of clay dispersion. Images a and b in Figure 6 reveal that VMT is mainly present as primary particles in the composite with no observable exfoliation or intercalation. The particles are about 0.5  $\mu\text{m}$ -thick and several micrometers long. Small cavities around the particles are believed to be created during microtoming of the 100 nm thick sections containing the rigid thick particles. These observations lead us to conclude that the absence of scattering peaks for PU\_VMT composites was largely due to the weak intensity of VMT reflections in the composite, rather than exfoliation. In contrast, CTAB-VMT particles in a PU composite, whose TEM images are shown in c and d in Figure 6, are delaminated into much smaller clay tactoids and exhibit a high degree of intercalation and exfoliation, in agreement with the above X-ray scattering results. Figure 6d shows exfoliated clay sheets with dimensions of  $<3$  nm in thickness and  $>100$  nm in length in the polyurethane matrix. The size reduction from VMT likely resulted from the exfoliation and sonication processes. As discussed above, the intercalated tactoids contributed to the scattering peak at  $2.3^\circ 2\theta$  and to the increased intensity at the low-angle region of the scattering pattern, while the exfoliated platelets would not contribute to defined X-ray scattering peaks.

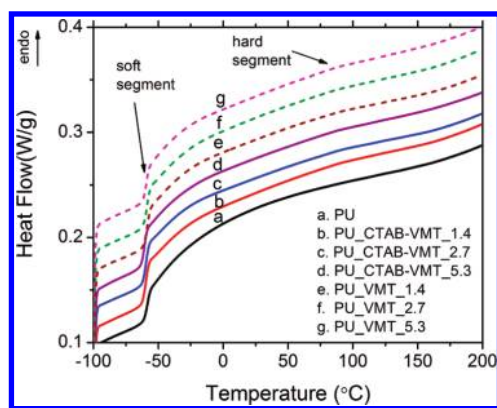


**Figure 7.** DSC curves of neat PU and PU-VMT composites. The glass transitions for the soft segments (SS) and the hard segments (HS) are indicated by arrows.

**Table 4.** Soft Segment  $T_g$  of Neat PU and Composites ( $^{\circ}\text{C}$ )

PU	PU_VMT (wt%)			PU_CTAB-VMT (wt%)		
	1.4	2.7	5.3	1.4	2.7	5.3
−58.2	−58.4	−58.6	−59.1	−59.6	−59.4	−60.6

Two factors may contribute to this intercalation-exfoliation mixed state. As indicated by its XRD pattern in Figure 2, the as-received vermiculite contains mica impurities, which have even higher charge densities and are therefore harder to exfoliate. From Figure 6c and 6d we can see that the intercalated clay tactoids are corrugated, but the stresses developed during the in situ polymerization are insufficient to break them apart completely. In contrast to Figure 6b, no cavities were observed in the thin sections because of the much smaller size of the delaminated particles.

**Thermal Properties of PU-VMT Nanocomposites.** The thermal properties of the PU-VMT composites were analyzed by DSC. The DSC traces are shown in Figure 7. The neat PU and the composite samples exhibit very similar low-temperature behavior, all showing a  $T_g$  around  $-58^{\circ}\text{C}$  to  $-60^{\circ}\text{C}$ , which is assigned to the glass transition of the soft segment in this polymer. The addition of the clay caused only a slight decrease in soft segment  $T_g$  as shown in Table 4, while it also led to the appearance of another feature around  $90^{\circ}\text{C}$ , which corresponds to the  $T_g$  of the hard segment. Similar behavior was previously observed by Chen et al.<sup>3</sup> A decrease in  $T_g$  after addition of clay has also been observed in epoxy-clay nanocomposites, and it has been argued that the organic modifier, which formed the interphase between the clay and the polymer matrix, can act as a plasticizer.<sup>42</sup> However, the composites with unmodified vermiculites also showed this behavior. It is generally considered that in polymer clay nanocomposites, an interphase forms between the hydrophilic clay surface and the polymer matrices, in which polymer components and functional groups on the clay surface interact strongly.<sup>43,44</sup> For PU, the hard segment has stronger interactions with the clay platelets through hydrogen bonding with siloxane oxygens or direct chemical bonding with silanol groups,<sup>43</sup> and thus the hard segment selectively concentrates at the interphase, inducing better microphase separation between soft and hard segments. Compared to neat PU, the soft-segment-rich domains within the composites contain fewer hard

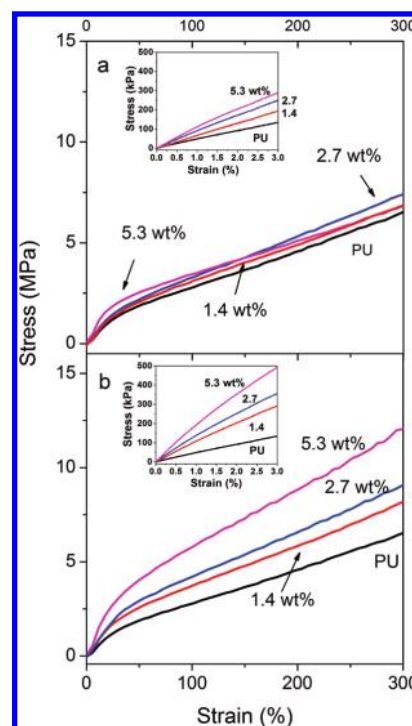


**Figure 8.** Stress–strain curves for neat PU and for PU composites with (a) VMT and (b) CTAB-VMT. Insets show the stress–strain curves for small strains.

**Table 5.** Mechanical Properties of the Neat PU and PU-VMT Composites

sample	tensile modulus (MPa)	tensile strength (MPa)	strain at break (%)
PU	$5.66 \pm 0.14$	$11.6 \pm 1.1$	$502 \pm 28$
PU_CTAB-VMT_1.4	$12.9 \pm 0.23$	$15.5 \pm 1.2$	$554 \pm 24$
PU_CTAB-VMT_2.7	$15.7 \pm 0.31$	$16.3 \pm 0.7$	$525 \pm 17$
PU_CTAB-VMT_5.3	$21.3 \pm 0.46$	$19.0 \pm 0.8$	$464 \pm 17$
PU_VMT_1.4	$8.13 \pm 0.24$	$10.3 \pm 0.9$	$542 \pm 20$
PU_VMT_2.7	$9.70 \pm 0.36$	$12.8 \pm 0.4$	$516 \pm 26$
PU_VMT_5.3	$13.2 \pm 0.55$	$11.0 \pm 0.6$	$498 \pm 23$

segments, so relaxation of those domains could occur at a lower temperature. The emergence of the hard segment endotherms in composites, features not found in the DSC trace of the neat PU, indicates that the clay induced partial condensation of hard segments; relaxation of the hard segments resulted in the observed endotherm. Even though the change in  $T_g$  of the soft segment was relatively small, the soft-segment  $T_g$  decreased slightly more for CTAB-VMT composites than for VMT composites, which could be due to the greater extent of exfoliation observed for the CTAB-VMT platelets, so that more clay surface was exposed to form the interphase.

**Mechanical Properties of PU-VMT Nanocomposites.** An important goal in forming polymer–clay nanocomposites is to achieve significant enhancements in mechanical properties with a clay content of only a few percent. According to the TEM observations, CTAB-VMT dispersed and exfoliated in PU much better than VMT, and as a consequence, platelets in this material have a much higher aspect ratio and show more remarkable



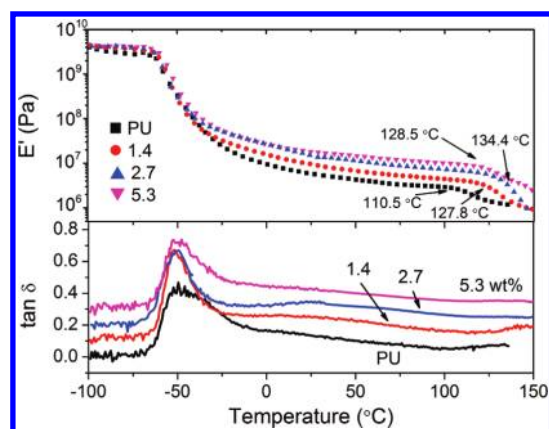


**Figure 9.** Dynamic mechanical analysis of the neat PU and PU\_CTAB-VMT composites. (a) Storage tensile modulus ( $E'$ ) and (b) loss factors ( $\tan \delta$ ) profiles.

effects in tensile properties, as demonstrated clearly by the stress–strain curves shown in Figure 8. The tensile modulus, tensile strength, and strain at break are summarized in Table 5. Both composites showed a steady increase in tensile modulus as clay content was increased, and the composites with CTAB-VMT showed much more significant improvement than those with VMT. At a loading of 5.3 wt % clay, the tensile modulus increased by 133% and 276% over neat PU for PU composites with VMT and CTAB-VMT, respectively. Adding VMT had little effect on tensile strength. In contrast, PU\_CTAB-VMT composites showed a significant increase in tensile strength from 11.6 to 15.5 MPa at 1.4 wt % and 19.0 MPa at 5.3 wt %. Despite the distinct difference in tensile strength, both composites showed a very similar trend in strain at break compared to neat PU, increasing slightly at first and then decreasing at 5.3 wt % of clay. However, different from thermoplastic PU systems, the composites here showed much less change in strain at break. In thermoplastic PUs, only physical cross-links (induced by phase separation of soft and hard segments) exist between linear polymer chains. In contrast, the thermoset composites synthesized here used a trifunctional polyol, capable of additional chemical cross-linking. The ultimate tensile behavior of these composites is dominated by the PU matrix, so that the strain at break is not affected much by the addition of clay.

Since the addition of CTAB-VMT induced significant increases in tensile modulus and tensile strength, it is worthwhile to examine the temperature dependence of the tensile modulus of the composite materials. These measurements were done by dynamic scanning tests from  $-100$  to  $150$  °C, and data are shown in Figure 9. The storage modulus of all the samples undergoes two distinct decreases as the temperature rises. The first decrease appears at around  $-50$  °C and corresponds to relaxation of the soft segment. Similar to the values of soft  $T_g$  measured by DSC, the peaks in  $\tan \delta$  for neat PU and for all the composites are very close, indicating that soft segment relaxation is insensitive to clay addition. The second decrease, however, is more different between neat PU and the composites. This relaxation did not produce a distinct peak in  $\tan \delta$  and the temperatures are close to, but higher than, the hard segment  $T_g$  observed in DSC measurements (Figure 7). No annealing step was employed in this test, so the second relaxation is caused by the rearrangement of hard segments. The relaxation temperatures for the composites are much higher than that of neat PU, but no clear trend was

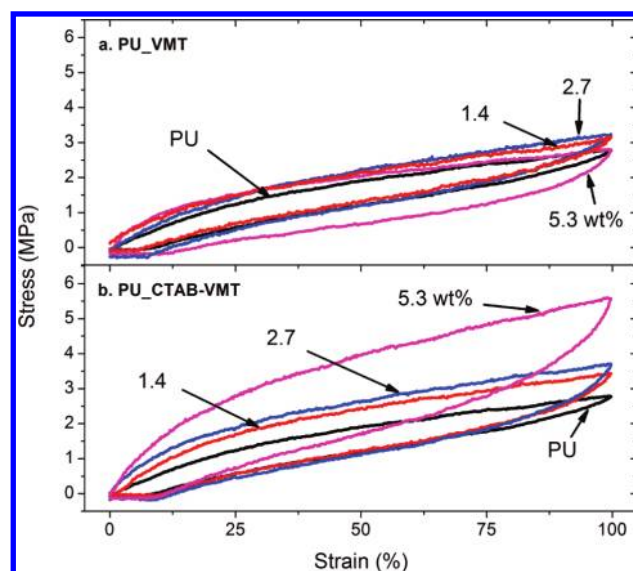


**Figure 10.** Hysteresis of the neat PU and composites in the first loading–unloading cycle.

**Table 6.** Hysteresis Properties of the Neat PU and PU-VMT Composites

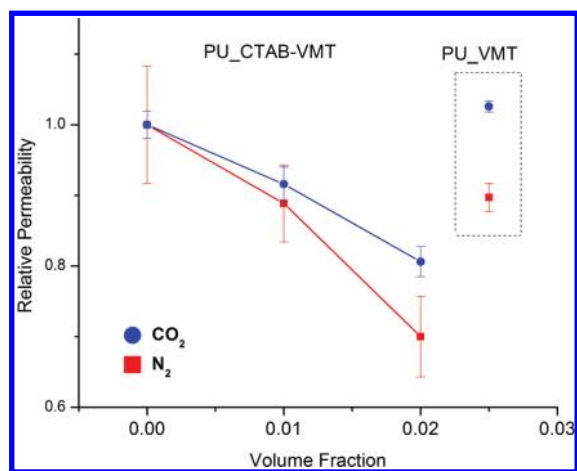
sample	hysteresis loss (%)		permanent set (%)
	first cycle	fifth cycle	fifth cycle
PU	31.8	14.1	6.6
PU_CTAB-VMT_1.4	43.4	20.5	10.9
PU_CTAB-VMT_2.7	51.3	24.5	11.6
PU_CTAB-VMT_5.3	49.6	21.5	11.9
PU_VMT_1.4	34.2	12.1	7.8
PU_VMT_2.7	40	20.4	9.4
PU_VMT_5.3	59.5	33.8	14.3

observed as a function of clay content. This change is similar to the observable DSC endotherms for hard segments in composites. This behavior is attributed to restricted motion of hard segments by surface tethering or intergallery confinement of clay sheets.

The incorporation of nanofillers into the polymer matrix affects the energy dissipation during the loading–unloading cycles, which is reflected in the hysteresis test. The hysteresis loss for the unfilled polymer is mainly attributed to crystallization, internal friction between polymer chains, breaking of hydrogen bonds, etc., and the resistance to deformation leads to unrecoverable strain, i.e., permanent set, after cycling.<sup>16</sup> On addition of nanoclay, the large interfacial interaction between the clay and the polymer matrix increases the internal friction, and the orientation of clay platelets also requires extra energy and increases the permanent set.<sup>45</sup> Figure 10 shows the hysteresis curve in the first cycle for neat PU and for the composites, and the hysteresis loss ratios in the first and fifth cycle. The permanent set values developed in the fifth cycle are listed in Table 6. A comparison between panels a and b in Figure 10 shows that for composites with VMT, the areas of the hysteresis loops did not change much compared to the neat PU, while for those with CTAB-VMT, the areas increased significantly. The permanent

**Table 7. CO<sub>2</sub> and N<sub>2</sub> Permeability Coefficients of Neat PU and PU-VMT Composites**

sample	$P_{\text{CO}_2}$ (Barrer)	$P_{\text{N}_2}$ (Barrer)
PU	104 ± 2	3.5 ± 0.3
PU_CTAB-VMT _2.7	95 ± 2.5	3.1 ± 0.2
PU_CTAB-VMT _5.3	84 ± 2	2.4 ± 0.2
PU_VMT_5.3	106 ± 1	3.1 ± 0.1

**Figure 11.** Plot of relative permeability of composite films as a function of the volume fraction of clay platelets.

set of the composites with CTAB-VMT increased compared to neat PU. The orientation of the clay platelets led to unrecoverable deformation. Although for the composites with VMT, the increase was relatively small at 1.4 and 2.7 wt %, it became even larger than for the CTAB-VMT counterpart at 5.3 wt %. This could be due to poor dispersion of VMT, so that at low content the deformation did not induce much orientation of the platelets, whereas at higher content, the orientation of large clay particles could lead to higher values of permanent set.

**Barrier Properties of PU-VMT Nanocomposites.** Compared to other high-aspect-ratio fillers, such as fibers or nanotubes, clay materials have sheetlike morphologies, and the platelets can act as diffusion barriers when they are incorporated in polymer composites. Carbon dioxide and nitrogen were used as model test gases to study the barrier properties of the composites, and composites with both unmodified VMT and CTAB-VMT were tested for comparison. The measured permeability coefficients are listed in Table 7 and the relative values compared to neat PU are plotted in Figure 11 against the volume fraction of the fillers (using densities of 2.3 g/cm<sup>3</sup> for the clay and 1.1 g/cm<sup>3</sup> for polyurethane). For the composites with CTAB-VMT, the permeability coefficient was reduced by 30% for N<sub>2</sub> and 19% for CO<sub>2</sub> at the highest volume fraction tested. For the same sample, the lower reduction in permeability of CO<sub>2</sub> observed here could be due to the higher solubility of CO<sub>2</sub> in the polyurethane-clay interphase than that of N<sub>2</sub>, since permeability is the product of diffusion coefficient and solubility. In contrast, for the composite with the same content of VMT (higher vol%), the permeability coefficient was reduced by 10.3% for nitrogen but increased a little for carbon dioxide. It has been argued that the permeability of polymer composites is dependent on a number of factors, such as the volume fraction, orientation, degree of dispersion, and

surface properties of the filler.<sup>46,47</sup> The first three factors affect the tortuosity of the path around clay particles as gas molecules pass through the film. Surface properties of the clay particles affect the interface in the composite, and an incompatible surface tends to create voids in the interfacial region, which can increase the free volume and consequently the permeability. Bearing the above factors in mind, the poor compatibility between VMT and PU led to little or no reduction in permeability, whereas the more compatible surface and greater extent of exfoliation of CTAB-VMT reduced the permeability significantly. The reductions in permeability obtained for PU-CTAB-VMT composites are similar to or exceed literature values for PU coatings, adhesives with montmorillonites,<sup>19,20,48</sup> or epoxy coatings with vermiculite.<sup>29</sup> The process of composite formation can affect the clay orientation, and differences are typically observed when a bar coater or shear forces are used. Solvent-based processes tend to result in better dispersion of clay, so it is expected that the permeability can be decreased even further with an optimal synthetic process and a higher clay content.

## CONCLUSIONS

Natural vermiculite was modified by exchange with quaternary ammonium cations, and XRD, FT-IR, and elemental analysis were used to monitor and characterize the modification process. The change in surface properties and increased interlayer spacings upon ion exchange resulted in better dispersion of the organoclay in polyether polyols. Significant shear-thinning effects were observed in all three polyols that were studied. The hydrophobicity of the polyol, represented by the EO:PO ratio, affected the intercalation of polyol into the clay interlayer space. The structure of the polyol was another important factor influencing the intercalation process. The polyol with EO-tips and PO-central blocks swelled the modified clays best and dispersions with CTAB-VMT showed the largest layer spacing and greatest shear thinning, and thus they were used for synthesis of PU composites.

TEM of PU composites with CTAB-VMT showed highly intercalated and partially exfoliated clay platelets, in contrast to the primary large clay particles in the composite with unmodified vermiculite. Compared to neat PU, a 276% increase in tensile modulus, a 64% increase in tensile strength and increased hysteresis were observed for PU-VMT composites with CTAB-VMT. The better dispersion state of the clay was crucial to improve the mechanical properties. The thermal properties did not change as much, probably due to incomplete exfoliation of clay, but increases in hard segment relaxation temperatures were observed in both DSC and DMA tests, suggesting strong interactions between hard segment and clay platelets. Better dispersion of clay platelets, combined with more the compatible surface of the organoclay to the polymer matrix, also induced greater reductions in the gas permeability coefficient.

## ASSOCIATED CONTENT

**S Supporting Information.** Elemental analyses and FT-IR spectra of pristine and modified vermiculite samples, stability and rheological properties of vermiculite-polyol dispersions, X-ray scattering data of Pluronic P123 dispersion with CTAB-VMT, and thermal stability data of PU-VMT nanocomposites. This



material is available free of charge via the Internet at <http://pubs.acs.org>.

## AUTHOR INFORMATION

### Corresponding Author

\*E-mail: [a-stein@umn.edu](mailto:a-stein@umn.edu) (A.S.); [macosko@umn.edu](mailto:macosko@umn.edu) (C.M.).

## ACKNOWLEDGMENT

The authors thank Huntsman Polyurethanes for providing financial support and Dr. Rafael Camargo and Dr. Qiang Lan from Huntsman for valuable discussions. The authors also thank Dr. David Giles and Mr. Yuanyan Gu for assistance in mechanical and gas permeation tests, respectively. Parts of this work were carried out in the University of Minnesota Characterization Facility, which receives partial support from the NSF through the NNIN program. Jeffol, Daltocel, and Suprasec are registered trademarks of Huntsman LLC and affiliates thereof in one or more, but not all countries.

## REFERENCES

- (1) Randall, D.; Lee, S. *The Polyurethanes Book*; John Wiley & Sons: New York, 2002.
- (2) Wang, Z.; Pinnavaia, T. J. *Chem. Mater.* **1998**, *10*, 3769–3771.
- (3) Chen, T. K.; Tien, Y. I.; Wei, K. H. *Polymer* **2000**, *41*, 1345–1353.
- (4) Jancar, J. *Polym. Compos.* **2000**, *21*, 369–376.
- (5) Sanchez-Adsuar, M. S.; Linares-Solano, A.; Cazorla-Amoros, D.; Ibarra-Rueda, L. J. *Appl. Polym. Sci.* **2003**, *90*, 2676–2683.
- (6) Koerner, H.; Price, G.; Pearce, N. A.; Alexander, M.; Vaia, R. A. *Nat. Mater.* **2004**, *3*, 115–120.
- (7) Kim, H.; Miura, Y.; Macosko, C. W. *Chem. Mater.* **2010**, *22*, 3441–3450.
- (8) Kojima, Y.; Usuki, A.; Kawasumi, M.; Okada, A.; Fukushima, Y.; Kurauchi, T.; Kamigaito, O. *J. Mater. Res.* **1993**, *8*, 1185–1189.
- (9) Okada, A.; Usuki, A. *Macromol. Mater. Eng.* **2006**, *291*, 1449–1476.
- (10) Nguyen, Q. T.; Baird, D. G. *Adv. Polym. Technol.* **2006**, *25*, 270–285.
- (11) Ma, J. S.; Zhang, S. F.; Qi, Z. N. *J. Appl. Polym. Sci.* **2001**, *82*, 1444–1448.
- (12) Rama, M. S.; Swaminathan, S. *J. Appl. Polym. Sci.* **2010**, *118*, 1774–1786.
- (13) Kim, W.; Chung, D. W.; Kim, J. H. *J. Appl. Polym. Sci.* **2008**, *110*, 3209–3216.
- (14) Rhoney, I.; Brown, S.; Hudson, N. E.; Pethrick, R. A. *J. Appl. Polym. Sci.* **2004**, *91*, 1335–1343.
- (15) Pattanayak, A.; Jana, S. C. *Polymer* **2005**, *46*, 3394–3406.
- (16) Xia, H. S.; Shaw, S. J.; Song, M. *Polym. Int.* **2005**, *54*, 1392–1400.
- (17) Berta, M.; Lindsay, C.; Pans, G.; Camino, G. *Polym. Degrad. Stab.* **2006**, *91*, 1179–1191.
- (18) Berta, M.; Saiani, A.; Lindsay, C.; Gunaratne, R. *J. Appl. Polym. Sci.* **2009**, *112*, 2847–2853.
- (19) Osman, M. A.; Mittal, V.; Morbidelli, M.; Suter, U. W. *Macromolecules* **2003**, *36*, 9851–9858.
- (20) Herrera-Alonso, J. M.; Marand, E.; Little, J. C.; Cox, S. S. *J. Membr. Sci.* **2009**, *337*, 208–214.
- (21) Pinto, U. A.; Visconte, L. L. Y.; Nunes, R. C. R. *Eur. Polym. J.* **2001**, *37*, 1935–1937.
- (22) Finnigan, B.; Jack, K.; Campbell, K.; Halley, P.; Truss, R.; Casey, P.; Cookson, D.; King, S.; Martin, D. *Macromolecules* **2005**, *38*, 7386–7396.
- (23) Roopa, S.; Siddaramaiah, A. *J. Reinf. Plast. Compos.* **2007**, *26*, 681–686.
- (24) Mishra, A. K.; Chattopadhyay, S.; Nando, G. B.; Devadoss, E. *Des. Monomers Polym.* **2008**, *11*, 395–407.
- (25) Xu, J.; Meng, Y. Z.; Li, R. K. Y.; Xu, Y.; Rajulu, A. V. *J. Polym. Sci., Part B: Polym. Phys.* **2003**, *41*, 749–755.
- (26) Lin, J. M.; Tang, Q. W.; Wu, J. H.; Sun, H. *Sci. Technol. Adv. Mater.* **2008**, *9*.
- (27) Slade, P. G.; Gates, W. P. *Appl. Clay Sci.* **2004**, *25*, 93–101.
- (28) Tjong, S. C.; Meng, Y. Z.; Hay, A. S. *Chem. Mater.* **2002**, *14*, 44–51.
- (29) Mittal, V. J. *Compos. Mater.* **2008**, *42*, 2829–2839.
- (30) Xie, Y. T.; Wang, A. Q. *J. Compos. Mater.* **2009**, *43*, 2401–2417.
- (31) Zhang, Y.; Han, W.; Wu, C. F. *J. Macromol. Sci., Part B: Phys.* **2009**, *48*, 967–978.
- (32) Patro, T. U.; Harikrishnan, G.; Misra, A.; Khakhar, D. V. *Polym. Eng. Sci.* **2008**, *48*, 1778–1784.
- (33) Harikrishnan, G.; Lindsay, C. I.; Arunagirinathan, M. A.; Macosko, C. W. *ACS Appl. Mater. Interfaces* **2009**, *1*, 1913–1918.
- (34) Osman, M. A. *J. Mater. Chem.* **2006**, *16*, 3007–3013.
- (35) Phillip, W. A.; Rzaev, J.; Hillmyer, M. A.; Cussler, E. L. *J. Membr. Sci.* **2006**, *286*, 144–152.
- (36) Mathieson, A. M. *Am. Mineral.* **1958**, *43*, 216–227.
- (37) Muiambo, H. F.; Focke, W. W.; Atanasova, M.; van der Westhuizen, I.; Tiedt, L. R. *Appl. Clay Sci.* **2010**, *50*, 51–57.
- (38) Amil, A. R.; Delacruz, F. A.; Vila, E.; Conde, A. R. *Clay Miner.* **1992**, *27*, 257–263.
- (39) Lindsay, C. I. WO/2003/059817, July 24, 2003.
- (40) Lu, Y.; Kong, S. T.; Deiseroth, H. J.; Mormann, W. *Macromol. Mater. Eng.* **2008**, *293*, 900–906.
- (41) Zhao, D. Y.; Feng, J. L.; Huo, Q. S.; Melosh, N.; Fredrickson, G. H.; Chmelka, B. F.; Stucky, G. D. *Science* **1998**, *279*, 548–552.
- (42) Chen, J. S.; Poliks, M. D.; Ober, C. K.; Zhang, Y. M.; Wiesner, U.; Giannelis, E. *Polymer* **2002**, *43*, 4895–4904.
- (43) Shi, H. Z.; Lan, T.; Pinnavaia, T. J. *Chem. Mater.* **1996**, *8*, 1584–1587.
- (44) Lu, H. B.; Nutt, S. *Macromolecules* **2003**, *36*, 4010–4016.
- (45) Finnigan, B.; Martin, D.; Halley, P.; Truss, R.; Campbell, K. *Polymer* **2004**, *45*, 2249–2260.
- (46) Choudalakis, G.; Gotsis, A. D. *Eur. Polym. J.* **2009**, *45*, 967–984.
- (47) George, S. C.; Thomas, S. *Prog. Polym. Sci.* **2001**, *26*, 985–1017.
- (48) Corcione, C. E.; Mensitieri, G.; Maffezzoli, A. *Polym. Eng. Sci.* **2009**, *49*, 1708–1718.